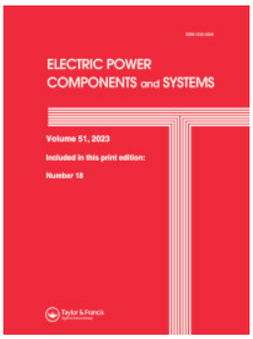

Taylor & Francis
Taylor & Francis Group

Electric Power Components and Systems

ISSN: 1532-5008 (Print) 1532-5016 (Online) Journal homepage: www.tandfonline.com/journals/uemp20

Design and Finite Element Analysis of a 6/4 Pole Multi-Layer Fully Pitched Switched Reluctance Motor to Reduce Torque Ripple

Cihan Sahin & Sinan Basaran

To cite this article: Cihan Sahin & Sinan Basaran (2023) Design and Finite Element Analysis of a 6/4 Pole Multi-Layer Fully Pitched Switched Reluctance Motor to Reduce Torque Ripple, Electric Power Components and Systems, 51:18, 2069-2084, DOI: 10.1080/15325008.2023.2205408

To link to this article: https://doi.org/10.1080/15325008.2023.2205408

Electric Power Components and Systems, 51(18): 2069–2084, 2023

ISSN: 1532-5008 print / 1532-5016 online
DOI: 10.1080/15325008.2023.2205408

Design and Finite Element Analysis of a 6/4 Pole Multi-Layer Fully Pitched Switched Reluctance Motor to Reduce Torque Ripple

Cihan Sahin [1] and Sinan Basaran [2]
[1]Department of Electric Program, Manisa Celal Bayar University, Technical Sciences Vocational School, Manisa, Turkey
[2]Department of Mechanical Engineering, Bilecik Seyh Edebali University, Faculty of Engineering, Bilecik, Turkey

CONTENTS

Abstract——In this study, the design and analysis of multi-layer fully pitched winding switched reluctance motor (MFP-SRM) for general use (submersible pump, electric vehicles, etc.) have been performed. It is seen that the multi-layer switched reluctance motor (SRM) has higher output power when compared to the single-layer SRM. In multi-layer SRM, the motors in the layers are electromagnetically independent of each other although they are identically the same motors with the same characteristics in terms of performance and geometry. Each layer of the MFP-SRM which is designed in this study consists of a 6/4 pole fully pitched SRM (FP-SRM) and these motors are magnetically independent of each other. In the MFP-SRM, which is designed as a double layer, there is a 15° phase difference between the rotor position angles and torque profile curves of each layer. With the phase difference that changes depending on the number of layers, each layer contributes to the total torque production of the profile, ensuring a smooth profile. According to the results of the 3D FEM analysis, it is seen that the proposed multi-layer motor structure has high starting torque and low torque ripple properties. In the analysis carried out in the range of 3–15 Amperes, the torque ripple of the traditional FP-SRM varies between 31.99% and 38.19%, while the torque ripple of the proposed MFP-SRM only varies between 3.23% and 7.11%.

1. INTRODUCTION

Switched reluctance motors consist of stators and rotors like conventional electric motors. SRMs generally have advantages such as low cost, reliability, durability, and high fault tolerance [1, 2]. These features ensure that SRMs are widely preferred in many applications such as wind turbines, electrical aircraft, and electric vehicles (EVs) [2]. Besides, they have been considered as a strong candidate for adjustable speed applications [3]. Even the SRMs are structurally similar to the stepper motors, on the contrary, they have fewer number of poles, larger stepping angles, and higher output power profiles [2]. Since SRM's stator and rotor structures have salient poles, they are also known as salient or double-salient

Keywords: multi-layer, fully pitched, switched reluctance motor, torque ripple, finite element analysis
Received 29 March 2021; accepted 31 January 2023
Address correspondence to Sinan Basaran, Department of Mechanical Engineering, Bilecik Seyh Edebali University, Faculty of Engineering, Bilecik, Turkey. E-mail: sinan.basaran@bilecik.edu.tr

motors [4].The main difference between their stator and rotor structure is that the phase windings are installed only at the stator poles. There are no windings or permanent magnets on their rotor [4]. This difference between rotor and stator constitutes the main structural principle of SRM. The fact that there is no winding used in the rotor of the SRM, it is shown that less copper is used, and there are fewer copper losses compared to other electrical machines [5]. SRMs have been shown as one of the alternative traction motors in EVs due to the absence of permanent magnets on their rotors [6, 7]. It has been reported that the amount of the production of EVs is increasing nowadays. This situation poses a future concern for the automotive industry due to the scarce supply of rare-earth permanent magnets [6]. Besides, demagnetization of the permanent magnets at high temperatures is a general problem for all motors which have magnets in their structure [8]. For these reasons, the main trend in traction motor selection has turned into the reduced magnet or permanent magnet-free motors, especially for automotive manufacturers [7]. Also, SRMs are more robust, easier to manufacture, and have lower cost rather than permanent magnet motors (PMM) which contain permanent magnets in their structure [4].

On the other hand, SRMs also have some disadvantages. High torque ripple is one of the major disadvantages of SRMs due to their high nonlinearity in torque production [9]. Since the stator and rotor of SRMs have salient poles, very high torque ripple phenomena occur during the phase commutation period. Consequently, these higher torque ripples produce acoustic noise, oscillations, and oscillation-oriented problems in SRMs [10, 11].

The problem of torque ripples has been greatly improved with the studies that have been carried out in recent years. SRMs torque ripple control methods can be divided into two groups: one is based upon machine design optimization and the other one is based upon control algorithms [3, 12]. In the first group, optimization studies are carried out on the geometric structure of the electric machine. To improve the magnetic characteristics of SRMs, geometric parameters (such as the stator and rotor pole arcs, air–gap length, number of poles, modifying the shape of rotor's or stator's salient poles) are adjusted to reduce the torque ripples [13, 14].

In the second group, different control techniques have been applied to reduce torque ripples [13, 14]. In the literature, there are different control methods such as instantaneous torque control, intelligent methods (fuzzy, neural network, etc.), and passivity-based adaptive sliding mode controllers that have been implemented to the system to reduce torque ripples [3, 15]. In this group of studies, there are not any modifications in the geometry of the electric machine.

Studies to improve the performance of SRMs have always been an area of interest for researchers. The most important point among these studies is based on the winding structure. The phase windings, which are wounded as short pitched per stator pole in conventional SRMs, are placed in full pitch by being distributed into the grooves in fully pitched SRMs. Although fully pitched SRMs have higher copper loss than conventional SRMs, due to their winding structure and working principle, they have higher torque density compared to conventional SRMs at an equivalent copper loss [16–18]. Approximately 20–30% more torque can be produced in a typical industrial frame [19]. However, the control algorithm of Fully pitched SRMs is more complex than conventional SRMs [20]. Despite this bottleneck, developments in control methods in recent years also increase the interest in fully pitched SRMs, which produce higher torque than conventional SRMs. Therefore, FP-SRM structure was preferred in this study.

This study aims to reduce the torque ripples of FP-SRMs and to obtain a smoother torque profile. For this purpose, a multi-layer fully pitched SRM (MFP-SRM) structure is proposed and the results of the numerical analysis for this structure are presented. Numerical methods are one of the well-known methods used to determine the magnetic field distributions of electrical machines [21]. When compared with the results obtained from analytical methods, it is seen that the results obtained from the numerical methods have higher accuracy. Therefore, numerical methods are more preferable tools by the researchers. The finite element analysis (FEA) tool is one of the most widely used numerical methods in electrical motor design [22].

The organization of this paper is as follows: In Section 2, basic concepts for traditional and fully pitched SRMs are given. In Section 3, the multi-layer SRM literature review and the proposed model MFP-SRM design are introduced. The working range of each layer of the proposed model MFP-SRM is determined in Section 4. In Section 5, magnetostatic analyzes which performed according to the determined working topology of MFP-SRM, and the results are presented. Finally, the evaluation of the study and the comments are given in the conclusion section.

2. CONVENTIONAL AND FULLY PITCHED SRM

Phase windings of SRMs are wounded as "short-pitched" around each stator pole as seen in Figure 1(a). Therefore,

conventional SRMs are also known as "Short Pitched-SRM" (SP-SRM). There are phase windings on each stator pole, and they are connected in series with the phase winding of the mutual stator poles. In this way, two stator poles create one phase of the motor [23]. As the number of stator poles increases in SRMs, the number of motor phases also increases.

In FP-SRMs, the phase winding is wrapped as "Fully-Pitched" as seen in Figure 1(b). A fully pitched winding structure was first proposed by Mecrow [23]. Mecrow changed the short-pitched winding structure to the full pitch to obtain higher torque than traditional SRMs. Proposed FP-SRM produces higher torque than traditional SRMs due to the fully pitched winding structure. While SP-SRMs are based on single-phase transmission, the FP-SRMs are based on two-phase transmission at the same time [17]. In FP-SRMs, the torque is produced by mutual inductance change between the phases in transmission [16, 23, 24]. Therefore, FPSRMs are also known as Mutually Couple Switched Reluctance Motor (MCSRM) [16, 23]. Figure 1 shows the 3-phase, 6/4-pole SP-SRM, and FP-SRM in 2D view. Also, Figure 2 shows the 3D view stator–rotor structure respectively for both motors.

For torque generation in SRMs, when any single phase is energized, the rotor moves in a direction that decreases the reluctance of the circuit. Continuity of rotor movement is provided by energizing the stator windings sequentially.

The electrical torque (T_e) produced by a single phase in SRMs depends on co-energy (W_c), and rotor position angle (θ). The expression of the electrical torque is given in Eq. (1) [17].

$$T_e = \left.\frac{\partial W_C}{\partial \theta}\right|_{i=const} \tag{1}$$

In a linear magnetic system, half of the electrical energy input is transformed into mechanical energy, also known as "co-energy", which is responsible for the generation of the mechanical torque. The other half, also known as "field energy", is stored on magnetic circuitry. In Figure 3, the current–flux linkage curve is given for linear magnetic systems [17].

As seen in Figure 3, co-energy, which expresses half of the electrical energy input in linear magnetic systems, is expressed with the equation given in (2) depending on the flux linkage (λ) and, current (i) [17].

$$W_c = \frac{1}{2}\lambda i \tag{2}$$

If it is assumed that two phases (a–b) are excited at the same time in the system, the co-energy expression given in Eq. (2) turns into Eq. (3) [17].

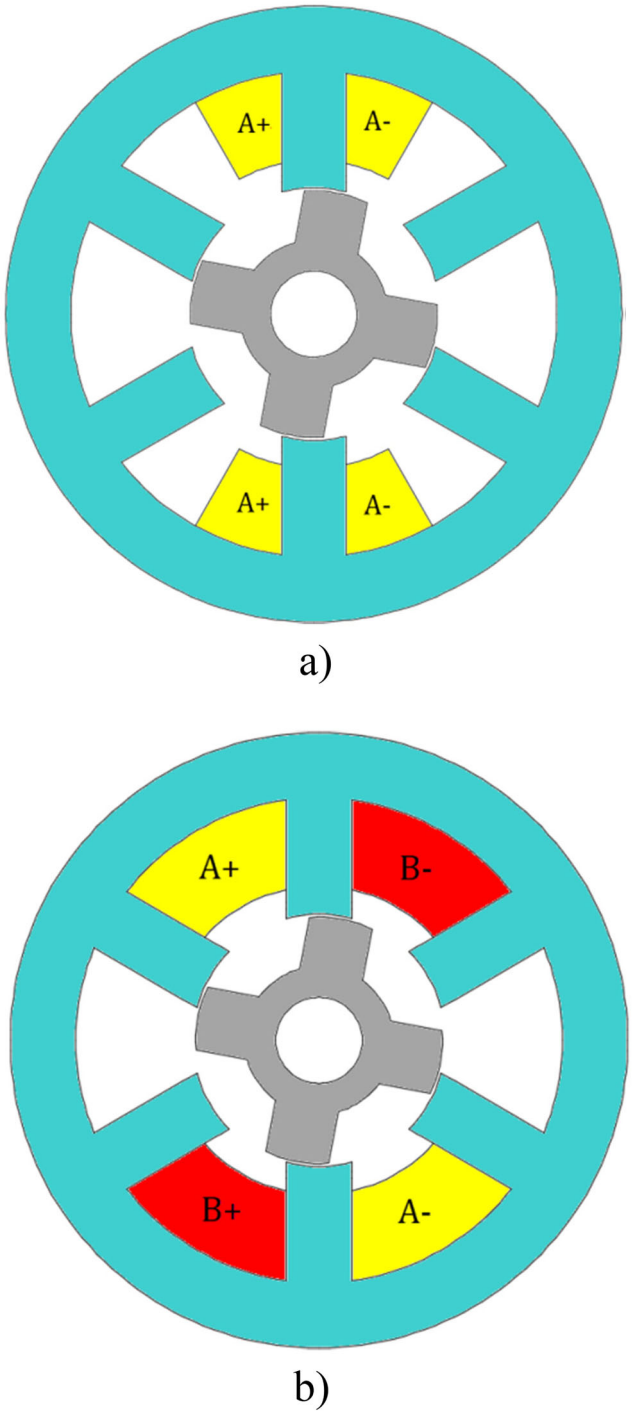

FIGURE 1. 2D view of 3 phase 6/4 pole motor: (a) SP-SRM, (b) FP-SRM.

$$W_c = \frac{1}{2}\,\lambda_a(\Theta,\ i_a,\ i_b)i_a + \frac{1}{2}\,\lambda_b(\Theta,\ i_a,\ i_b)i_b \tag{3}$$

Flux linkages containing self-inductances and mutual inductances can be expressed as a function of phase currents, and rotor position. λ_a and λ_b are vary depending on

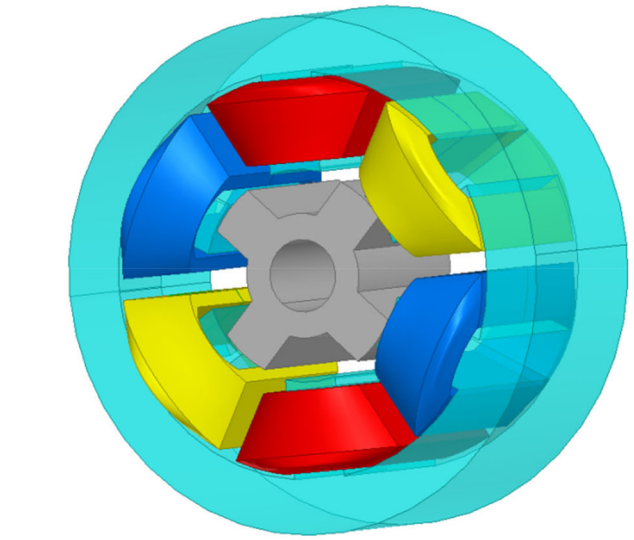

a)

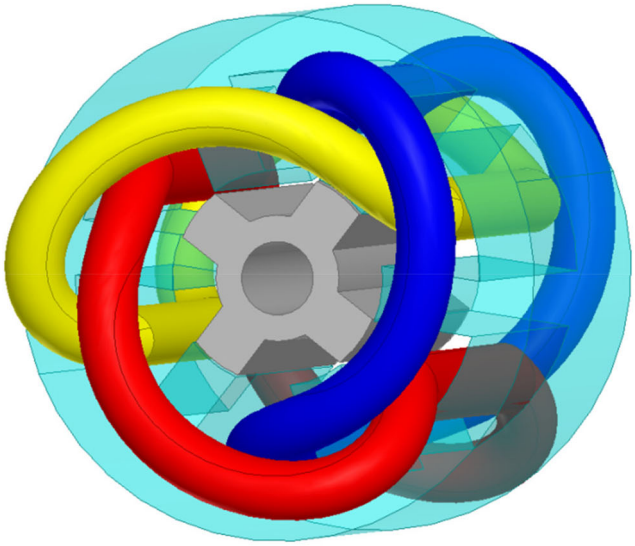

b)

FIGURE 2. 3D view of 3 phase 6/4 pole motor: (a) SP-SRM, (b) FP-SRM.

phase currents, self-inductance, and mutual-inductance given in Eqs. (4) and (5), respectively [17].

$$\lambda_a(\Theta,\ i_a,\ i_b) = i_a L_a + i_b M_{ab} \tag{4}$$

$$\lambda_b(\Theta,\ i_a,\ i_b) = i_b L_b + i_a M_{ab} \tag{5}$$

Here, L_a, L_b are the self-inductances of phases a and b, respectively, and M_{ab} is the mutual inductance that occurs between phases a and b. If the λ_a and λ_b equations given in

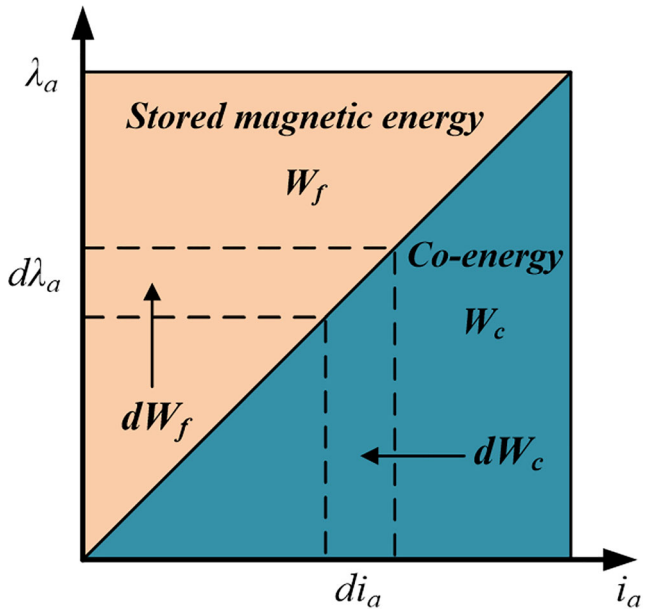

FIGURE 3. Flux linkage–current for a linear magnetic system [19].

(4) and (5) are replaced in Eq. (3), the co-energy expression turns into the equation given in (6) [17].

$$W_c = \frac{1}{2}\left(L_a i_a^2 + L_b i_{b+}^2 2 i_a i_b M_{ab}\right) \tag{6}$$

If the co-energy expression given in Eq. (6) is replaced in Eq. (1), the torque expression is obtained as given in (7). If three phases (a, b, c) are assumed to be in a conduction state, the electrical torque term turns into (8). Here, L_c refers to the self-inductance of the c phase, M_{bc} refers to the mutual inductance between phases b and c, and M_{ca} refers to the mutual inductance between phases c and a [17].

$$T = \frac{1}{2} i_a^2 \frac{\partial L_a}{\partial \theta} + \frac{1}{2} i_b^2 \frac{\partial L_b}{\partial \theta} + i_a i_b \frac{\partial M_{ab}}{\partial \theta} \tag{7}$$

$$T = \frac{1}{2} i_a^2 \frac{\partial L_a}{\partial \theta} + \frac{1}{2} i_b^2 \frac{\partial L_b}{\partial \theta} + \frac{1}{2} i_c^2 \frac{\partial L_c}{\partial \theta} + i_a i_b \frac{\partial M_{ab}}{\partial \theta} + i_b i_c \frac{\partial M_{bc}}{\partial \theta} + i_c i_a \frac{\partial M_{ca}}{\partial \theta} \tag{8}$$

In FP-SRMs, to obtain mutual inductance between phases, each phase contributes 2/3 of the energization period for effective torque generation, since two-phase windings must be energized at the same time [23]. This situation also makes it difficult to control FP-SRMs. However, this problem has been resolved to a great extent with the control methods developed in recent years. In FP-SRMs, the torque equation takes the form given in Eq. (9)

because self-inductance is neglected [16].

$$T = i_a i_b \frac{\partial M_{ab}}{\partial \theta} + i_b i_c \frac{\partial M_{bc}}{\partial \theta} + i_c i_a \frac{\partial M_{ca}}{\partial \theta} \tag{9}$$

Since each phase contributes 1/3 to the torque produced in SP-SRM and 2/3 in FP-SRM, copper losses are expressed with Eq. (10) for SP-SRM and Eq. (11) for FP-SRM. FP-SRM phase resistance is 59–62% higher than SP-SRM. If this ratio is accepted as 62%, the resistance coefficient $R_{fp} = 1.62R_{sp}$ can be written [25]. Here, R_{sp} represents the phase winding resistance of the SP-SRM and R_{fp} represents the phase winding resistance of the FP-SRM. Equations (10) and (11) should be equalized to each other to make comparisons in equivalent copper losses. The equation given in (12) has been obtained with Eqs. (10) and (11) by using the resistance coefficient.

$$P_{sp} = \frac{1}{3} i_{sp}^2 R_{sp} \tag{10}$$

$$P_{fp} = \frac{2}{3} i_{fp}^2 R_{fp} \tag{11}$$

$$i_{fp} = 0.559 i_{sp} \tag{12}$$

In these equations, P_{sp} represents the copper loss, i_{sp} represents the phase current of the SP-SRM, P_{fp} represents the copper loss and i_{fp} represents the phase current of the FP-SRM for unipolar excitation. As can be seen from Eq. (12), FP-SRMs show higher performance at a lower current (equivalent copper loss) than conventional SRMs.

3. MULTI-LAYER SRMs

Multi-layer structure is an approach used to reduce the torque ripple of SRMs. In recent years, several SRM studies with different multi-layer structures have been conducted [26]. Multi-layer SRMs consist of multiple layers that are completely independent magnetically from each other but have the same performances and properties. Motors in each layer contribute to the output torque in different positions. When the literature is examined for multi-layer SRMs, a fully pitched winding structure is not encountered. In the study conducted by Seshadri et al., it is stated that the multi-layer structure helps to reduce torque ripple by 23% [27]. Vahedi et al. [28] presented a fast and simple magnetic equivalent circuit (MEC) model for single-layer classical SRM. It has been suggested that this presented model can be used in multi-layer SRMs. In the study, 2, 3, 4, and 5-layer 6/4, 8/6, and 12/8 SRM structures were examined. In the simulation studies performed for the 2-layer 6/4 SRM structure, it was observed that the torque ripple value decreased from 155.34% to 43.1%. In the study conducted by Siadatan et al. where a seven-layer 4/4 pole classical SRM with high torque/volume density called septi segment SRM (SSSRM) [29]. Afjei et al. have conducted a modeling and prototype study for a motor structure called quintuple-set SRM (QSSRM) for high torque/ripples and high torque/volume applications [30]. They used the five-layer 4/4 pole classical SRM structure in the proposed structure. In the study of Siadatan et al., a double layer 6/4 pole classic switched reluctance motor/generator (SRM/G) structure was designed [31]. The most important point of the study is that it offers a hybrid operating mode with both motor and generator modes. A novel three-phase seven layers switched reluctance motor (SLSRM) was designed in the study conducted by Afjei et al. [32]. The motor used in the study has 4/4 poles and has a classical SRM winding in each layer. In the study conducted by Torkaman et al. high torque and low-flux-leakage SRM models were proposed [33] The model subject to the study is called DLPISRM (double-layer-per-phase-isolated SRM). In the study performed by Dalbadan et al. double-layer MSRM (multi-layer switched reluctance motor) was designed by using a 6/4 pole classical SRM structure [34] According to the test and simulation results obtained, it has been shown that the multilayer motor structure has high starting torque, less acoustic noise, and a smooth torque profile. Due to the reduction in the torque ripple, the acoustic noise values of the motor have decreased. Classical SRM noise pressure is measured between 72.54 and 56.55 (dBA) for different operating speeds up to 3000 rpm, while the recommended multi SRM is measured between 70.43 and 52.88 (dBA). In 2002, a study conducted by Afjei and Toliyat [35] was reported as the first multi-layer SRM design [34] A three-layer structure has been proposed in the work they carried out. All layers in the proposed structure have a conventional winding structure. Similarly, the classical SRM structure was used in the studies performed in [36–41].

As can be seen from the literature review carried out, FP-SRMs with full pitch winding structures were not used in multi-layer designs. One of the most important reasons for this is that FP-SRMs are difficult to control due to the two phases being activated at the same time. However, control techniques developed in recent years significantly exceed this challenge.

3.1. Description of the Proposed MFP-SRM (Multi-Layer Fully-Pitched Switched Reluctance Motor)

The proposed model has a double-layer FP-SRM structure with 6/4 poles on each layer. The 6/4 combination is the

most basic structure in SRM. Therefore, it is the most suitable combination of slots/poles for the theoretical evaluation of a new design [42]. The proposed structure of a two-layer, fully-pitched switched reluctance motor (MFP-SRM) is given in Figure 4. In the MFP-SRM model, all layers are connected on the same shaft and contributing to the output torque in their operating range. Since all layers have the same geometric dimensions, the geometric parameters of FP-SRM in the layers in Figure 5 are given in 2D.

As given in Figure 5, β_r represents the rotor pole arc (degree), β_s is the stator pole arc (degree), t_s is the stator pole width, t_r is the rotor pole width, d_s is the stator pole height, d_r is the rotor pole height, y_s is the stator yoke thickness, y_r is the rotor yoke thickness, and g is the air–gap length. Geometric dimensions of FP-SRM are given in Table 1. Also, nominal parameters of MFP-SRM are given in Table 2. Matlab GUI based SRM design program was used to find motor parameters [43].

4. DETERMINING THE WORKING RANGE OF MFP-SRM LAYERS

In this section, to determine the working range of the layers, firstly, the torque profile of FP-SRM in each layer has been obtained. Since different layers have the same performances in multi-layer SRMs, it is sufficient to examine a single layer for motor performance prediction. For this, magnetostatic analysis of FP-SRM in a single layer for different current values using the finite element method was performed. Accurate estimation of motor performance is very important in design optimizations. However, due to the inherent nonlinearity of SRMs, it is very difficult to obtain a practical mathematical model. Therefore, various methods such as the finite element method (FEM), magnetic equivalent circuit (MEC), neural networks, and fuzzy inference systems are used to improve the approximation accuracy of nonlinear features [44]. Although a full electrical model and control system is needed to evaluate the dynamic behavior, the verification of the model accuracy is also obtained by using the FEM method [45]. Furthermore, FEM analysis is essential in SRMs because of their double salient structure and the intense saturation effects that arise in the partially aligned stator-rotor poles [46]. In FEM, necessary profiles such as torque, magnetizing, self-inductance, and mutual inductance are obtained for the analysis and modeling of SRMs based on changes in phase current and rotor position using Maxwell's equations. These profiles can be calculated using the flux density B and field intensity H by utilizing a set of Maxwell equations [47].

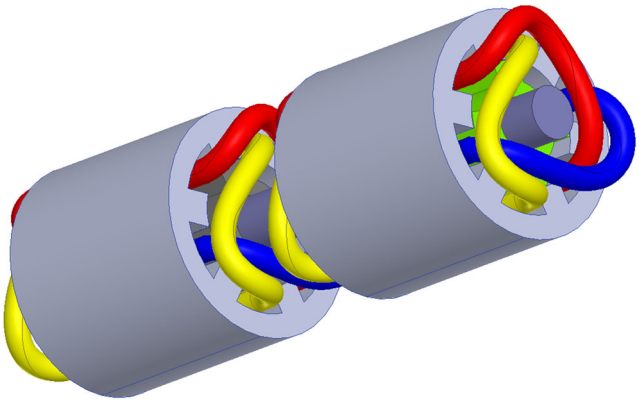

FIGURE 4. Two layer fully-pitched switched reluctance motor (MFP-SRM).

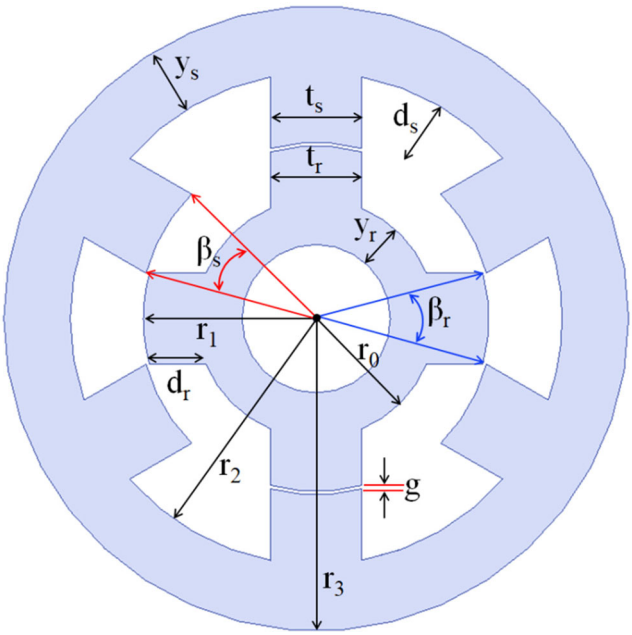

FIGURE 5. Geometric parameters of the FP-SRM.

Symbol	Value	Symbol	Value
r_0	17.6 (mm)	y_s	9.8 (mm)
r_1	25.5 (mm)	y_r	6.65 (mm)
r_2	36.3 (mm)	d_s	10.3 (mm)
r_3	46.1 (mm)	d_r	7.9 (mm)
t_s	13.46 (mm)	β_r	30^0
t_r	13.46 (mm)	β_s	30^0
g	0.50 (mm)	depth	90.00 (mm)

TABLE 1. Geometric dimensions of the FP-SRM.

The 2D-FEM analysis computation times are shorter than the 3D-FEM analysis computation times, but the coil-end effect in 2D-FEM analyzes cannot be included in the calculation. This situation causes a slight decrease in the output torque calculations [48]. Also, 3D-FEM analysis has been preferred to examine the torque effect of each layer on the shaft in multi-layer SRMs more accurately. Figure 6(a) shows the torque profile obtained as a result of 3D-FEM analysis of each layer of MFP-SRM performed at different currents, and Figure 6(b) shows the mutual inductance profile of each layer of the MFP-SRM.

In multi-layer SRMs, the instantaneous torque can be generated from the sum of instantaneous torques in different layers. In traditional multi-layer SRMs, the instantaneous torque can be obtained by multiplying the torque produced in a layer by the total number of layers. However, in this case, the torque ripple of conventional multi-layer SRM and single layer SRM will be the same [28]. To eliminate this situation, the rotors are positioned

Nominal parameters of MFP-SRM

Layer number of MFP-SRM	2
Each layer stator/rotor pole numbers	6/4
Number of phases	3
Rated current (Amps)	10
Rated power (W)	2250
Rated speed (rpm)	1750

TABLE 2. Nominal parameters of MFP-SRM.

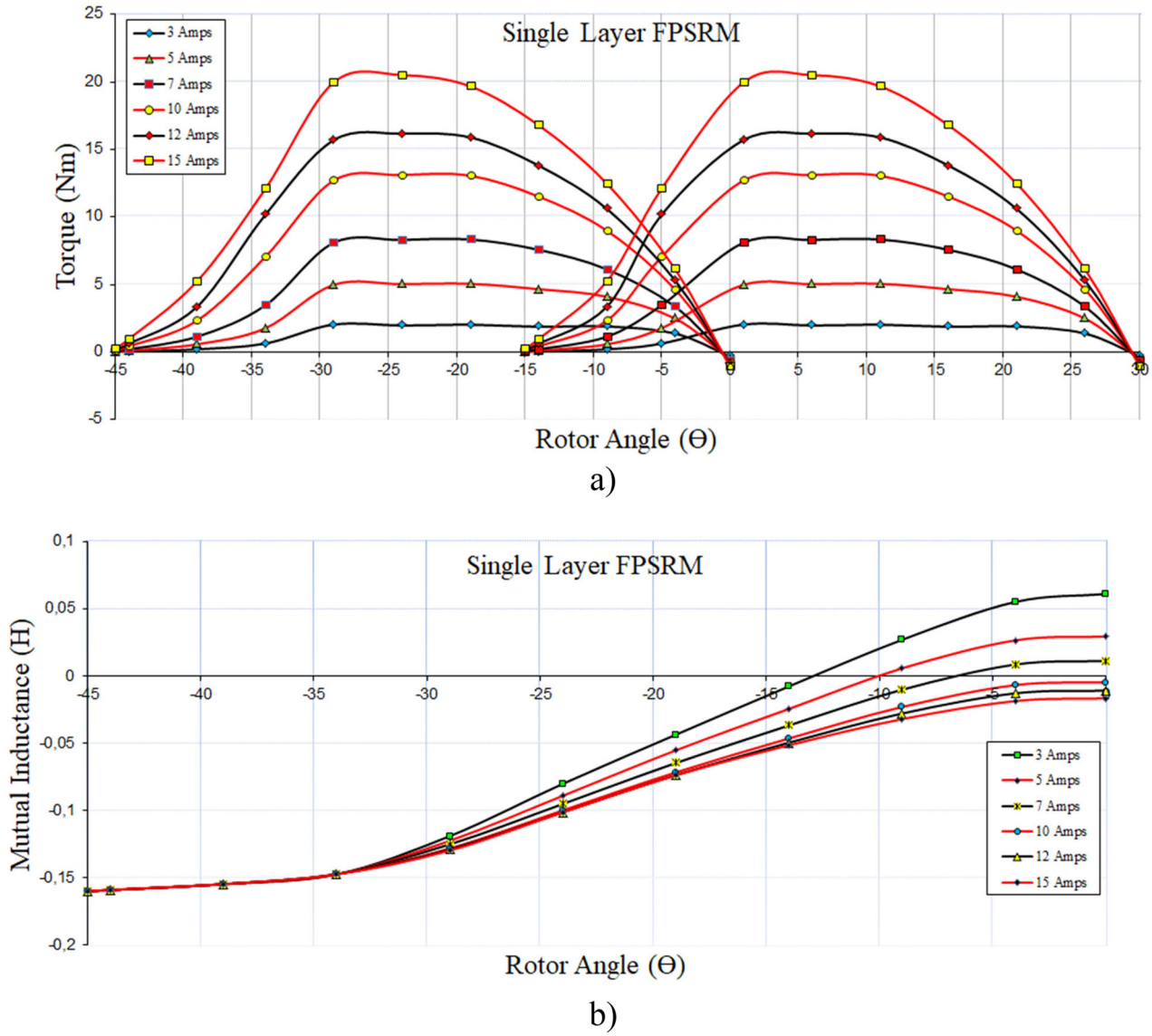

FIGURE 6. Results for a single layer of MFP-SRM at different currents: (a) torque profiles (b) mutual inductance profiles.

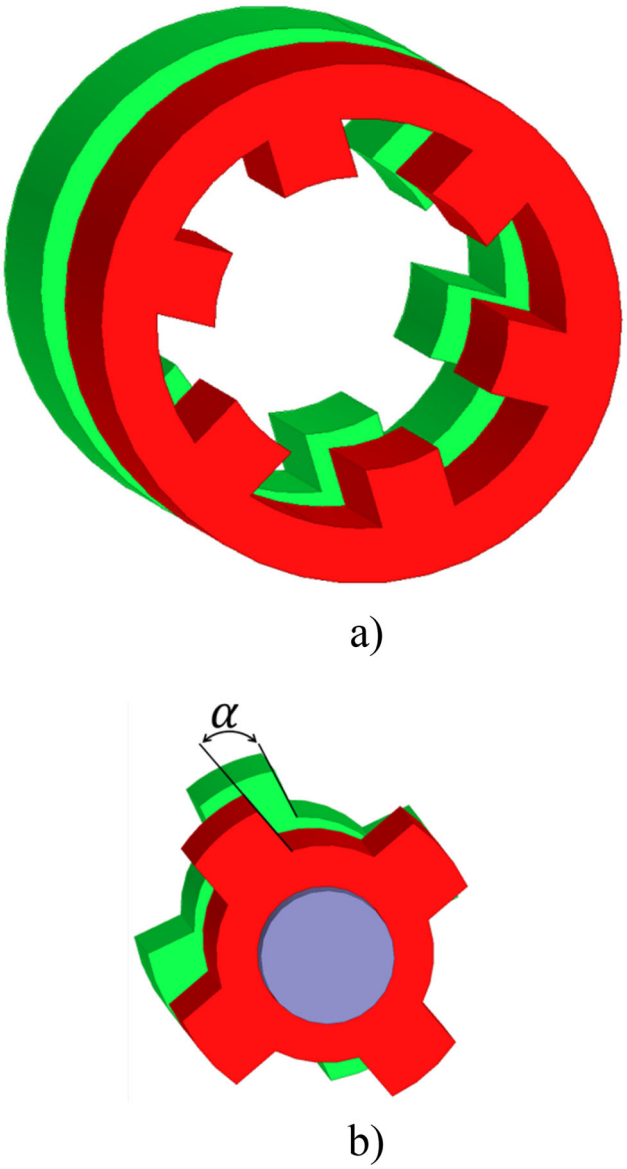

FIGURE 7. The structure proposed for the multi-layer: (a) stator, (b) rotor.

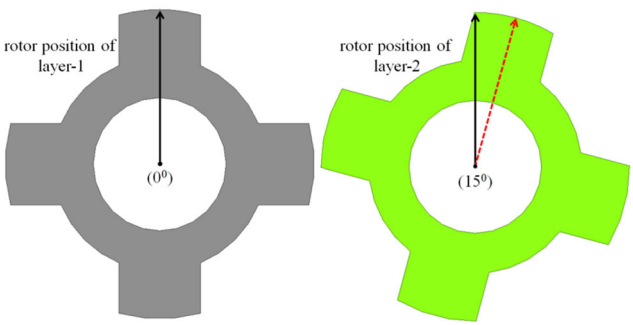

FIGURE 8. Position angle difference between rotor layers.

so that there is a certain angular displacement between them, as shown in Figure 7. In this way, a time shift is created between the torque waveforms produced in the layers. As a result of this situation, a significant improvement is provided in torque ripples in multi-layer SRMs [28]. Equation (13) is used to determine the optimum value of the angle α [28]

$$\alpha = \frac{360^0}{P_r N_{phase} N_{layer}} \tag{13}$$

In Eq. (13), P_r represents the number of rotor poles, N_{phase} the number of phases, and N_{layer} the number of layers. If the phase number ($N_{phase} = 3$), layer number ($N_{layer} = 2$), and rotor pole number ($P_r = 4$) of the designed MFP-SRM are replaced in Eq. (13), the α value is found as 15°. In this case, the rotor positions in both layers are as given in Figure 8 and the torque profile curves are presented in Figure 9. The torque profiles are given in Figure 9 obtained at 5 Amps where time shift occurs between instantaneous torque of layers.

After determining the phase difference between the rotor layers, the most important point to be considered is to determine the energization time of the relevant phase windings that the MFP-SRM in each layer will contribute to the torque generation.

In case the phase windings of both layers are energized at the same time, the output torque will be negatively affected as it is the total torque. To prevent this, the time shift must be taken into account when the phase windings of the second layer are energized. For the torque generation of both layers, the phase windings are energized in the same way and only differ in timing. When two phases (a–b) of the first motor are energized for torque generation; Two phases (a–b) of the second layer must be energized afterward at an angle α. Due to this difference, a different driver must be used for each layer.

For the suggested MFP-SRM model in Figure 9, torque generations of both layers are seen which is based on the time shift angle. In this work, each motor model for both layers is energized depending on the time shift, and that contributes to the maximum torque generation. For this, after providing the startup torque of the first motor, the time interval for transmission is determined for each layer. In determining the time interval, the torque graphs given in Figure 9 depending on the time shift were used. The angle values where the torque curves of both layers intersect have been chosen as the reference point. To precisely determine the intersection points, the magnetostatic analysis of each layer was performed independently with 0.5°

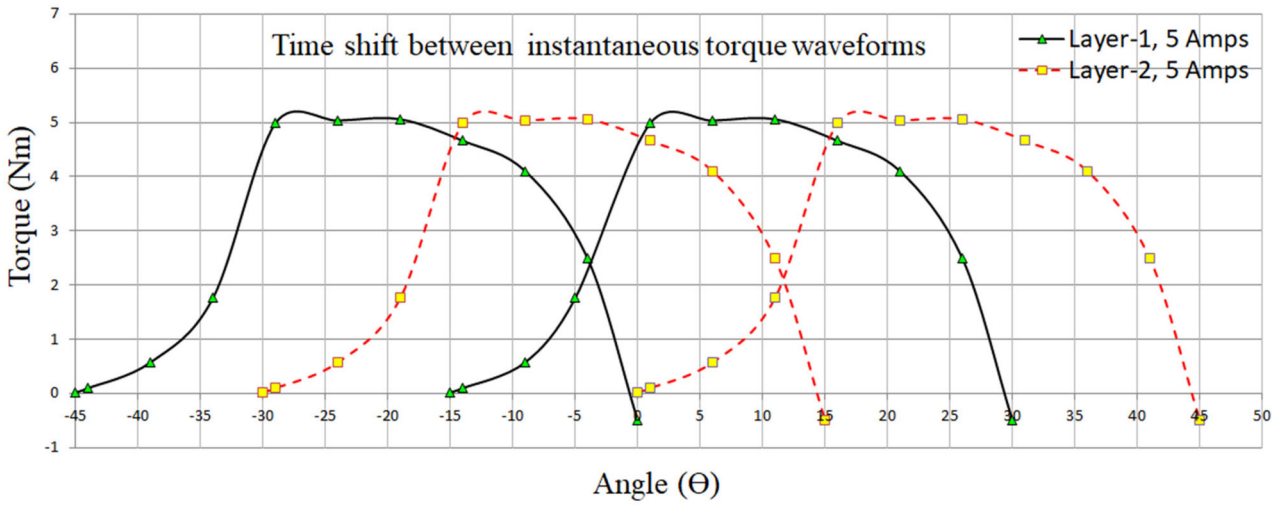

FIGURE 9. The time shift between instantaneous torque of layers.

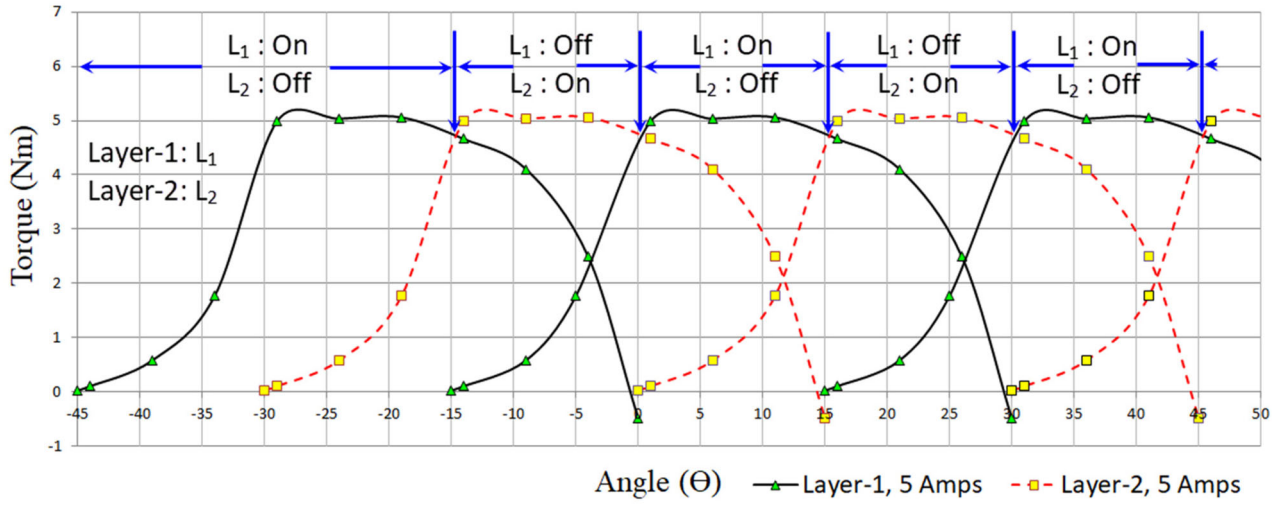

FIGURE 10. Working range of layers.

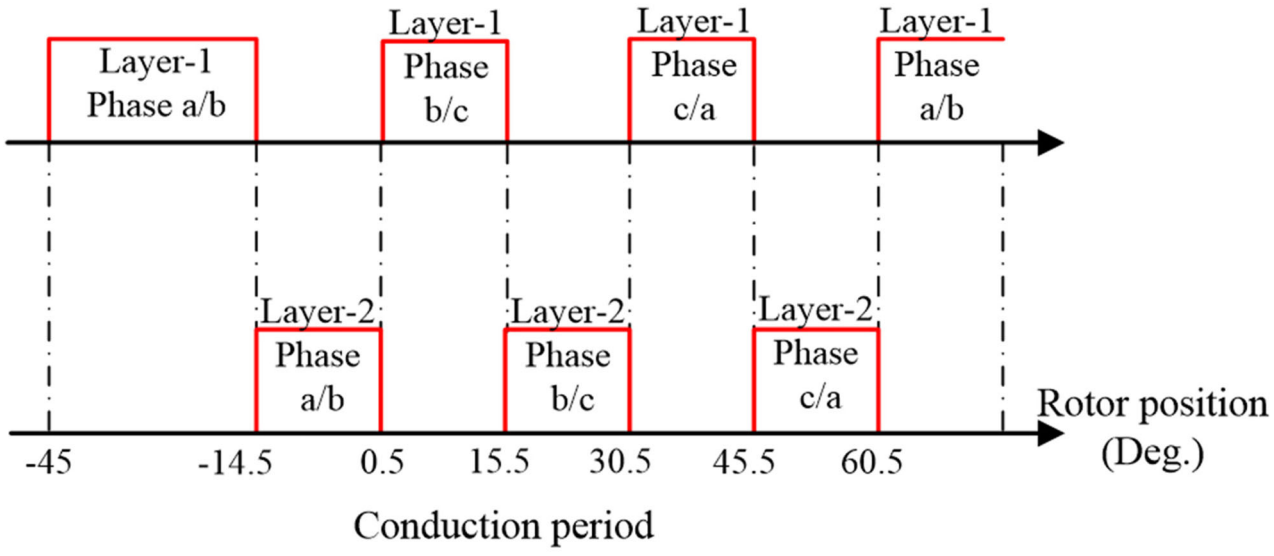

FIGURE 11. The energization period of layers and phases.

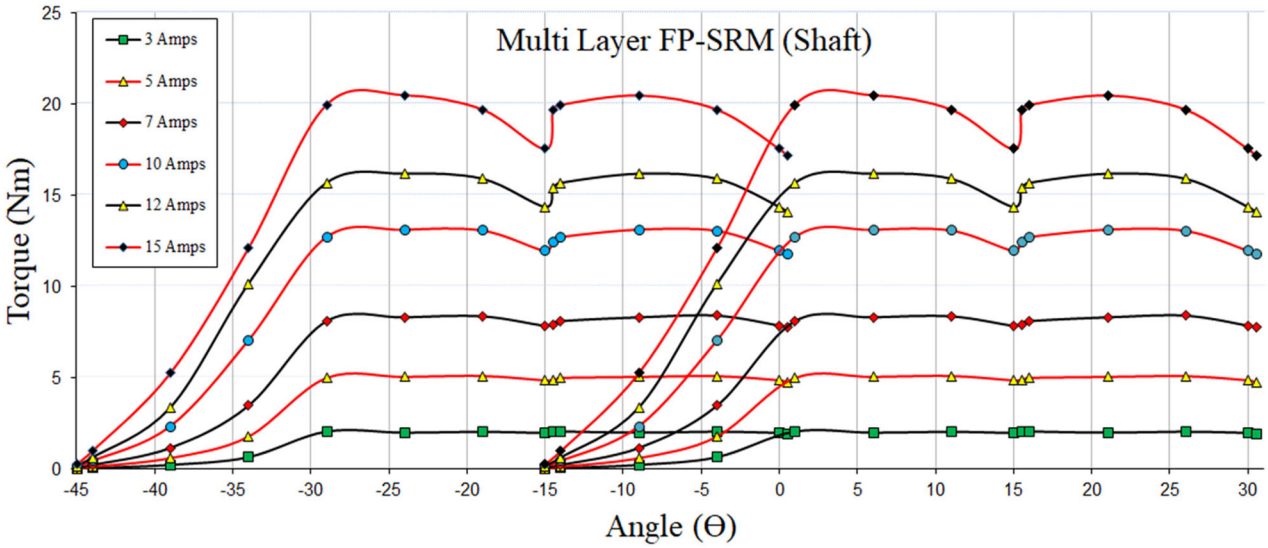

FIGURE 12. MFP-SRM torque curves.

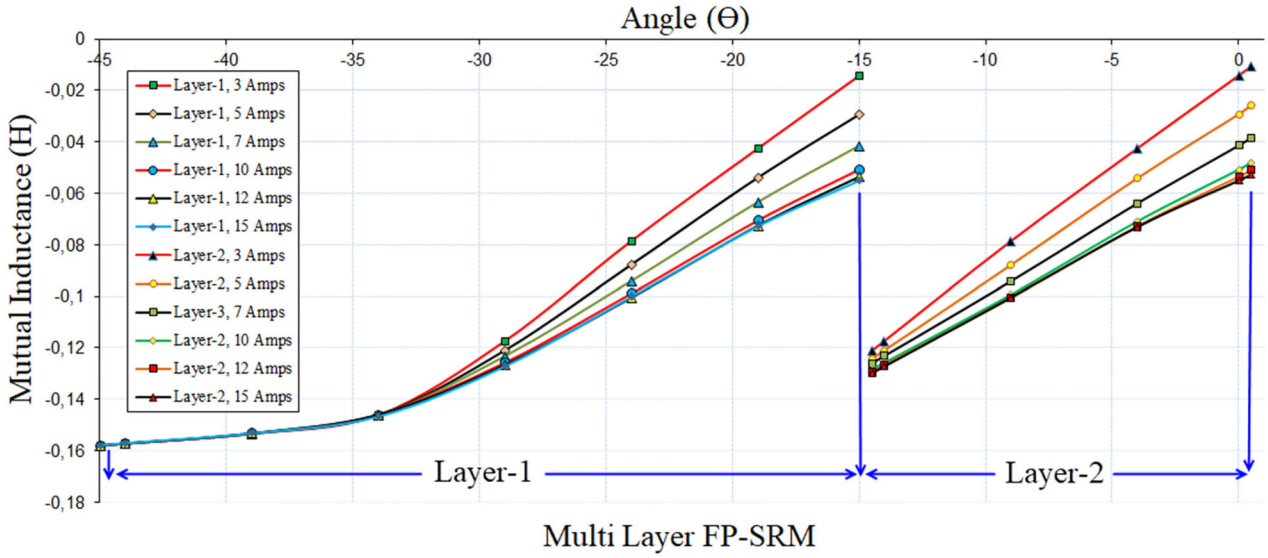

FIGURE 13. MFP-SRM mutual inductance curves.

steps in the regions close to the intersection points of the torque curves. As a result of the finite element analysis, the working range is given in Figure 10 and the phase energizing sequence given in Figure 11 was obtained.

5. MAGNETOSTATIC ANALYSIS AND RESULTS OF MFP-SRM

To compare the output torque curves of the proposed model MFP-SRM and classical FP-SRM, 3D FEM analysis was performed at different currents in both models. The torque curves of the classical FP-SRM were given in Figure 6. In MFP-SRM, all layers contribute to the output torque at maximum torque generation points (Figures 10 and 11). In this way, a smoother torque curve can be obtained in MFP-SRM compared to classical FP-SRM. The analyses of the proposed model MFP-SRM and the FP-SRM whose results are given in Figure 6 were carried out under the same conditions to compare the results accurately. Figure 12 shows the angle-torque results obtained from the magnetostatic analysis of MFP-

SRM between 3 and 15 Amperes. Each layer was generating torque and contribute to the output torque according to Figures 10 and 11.

Torque generation in FP-SRMs is produced depending on the mutual inductance between active phases. In the proposed model MFP-SRM, the relevant phases of each

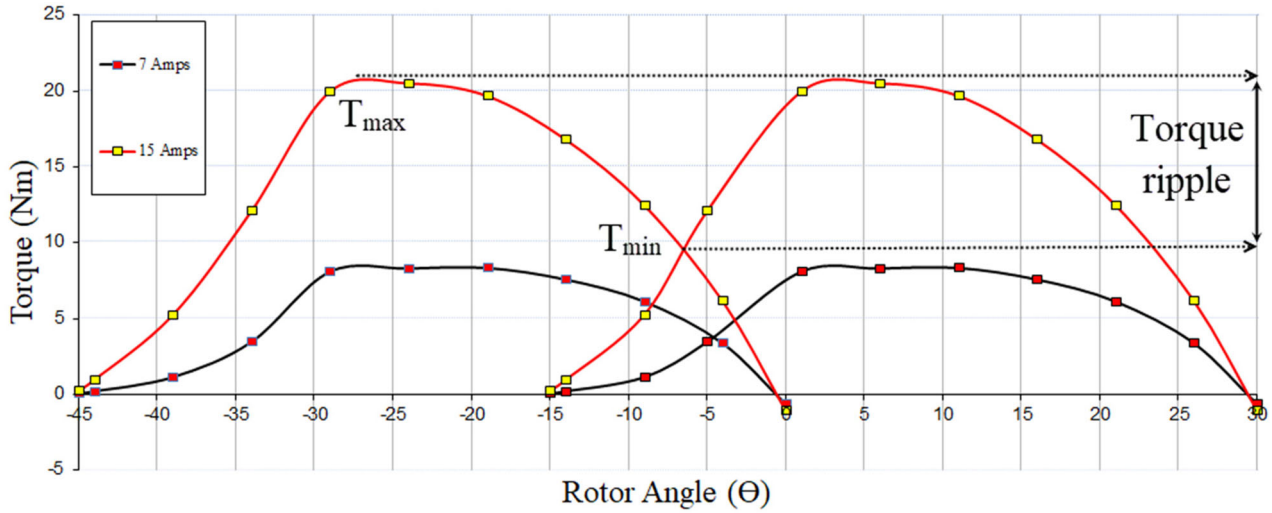

FIGURE 14. Classical FP-SRM torque ripple curve.

	FP-SRM				MFP-SRM				Variation	
Current (Amps)	T_{avg} (Nm)	T_{rip} (%)	P_{out} (W)	Efficiency η (%)	T_{avg} (Nm)	T_{rip} (%)	P_{out} (W)	Efficiency η (%)	Δ % T_{ripple}	Δ T_{avg}(%)
3	1.54	31.99	282.06	86.2	1.98	3.23	362.65	88.9	–28.76	+28.57
5	3.72	35.96	681.35	91.6	4.90	3.56	897.48	93.5	–32.4	+31.72
7	6.03	38.19	1104.45	81.8	8.03	4.03	1470.77	85.7	–34.16	+33.16
10	9.63	36.01	1768.83	77.9	12.48	5.04	2285.83	82.1	–30.97	+29.59
12	11.99	34.78	2169.08	75.3	15.30	5.75	2802.34	79.6	–29.03	+27.61
15	14.94	37.14	2736.41	70.8	19.11	7.11	3500.18	75.6	–30.03	+27.91

TABLE 3. T_{avg}, T_{rip}, P_{out} and efficiency comparisons of conventional FP-SRM and MFP-SRM.

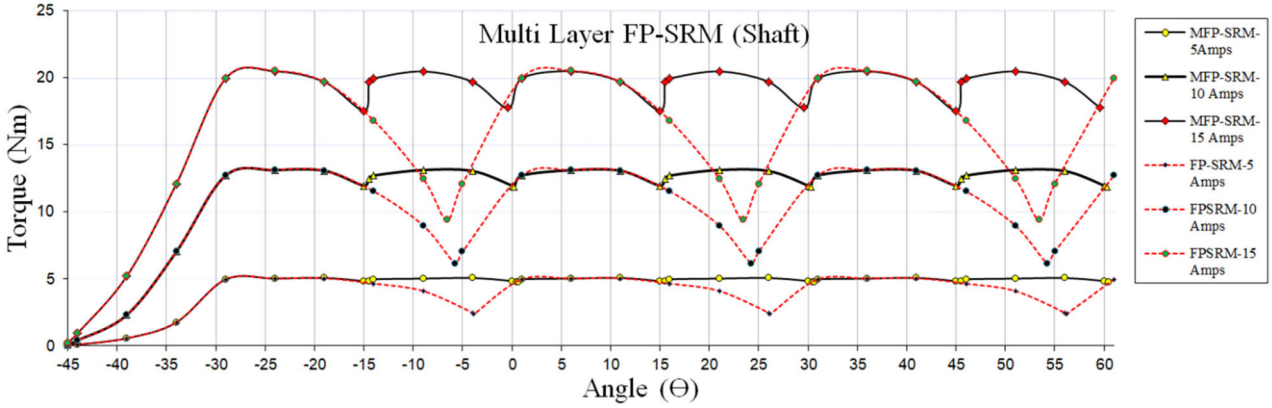

FIGURE 15. Comparison of FP-SRM and MFP-SRM torque curves.

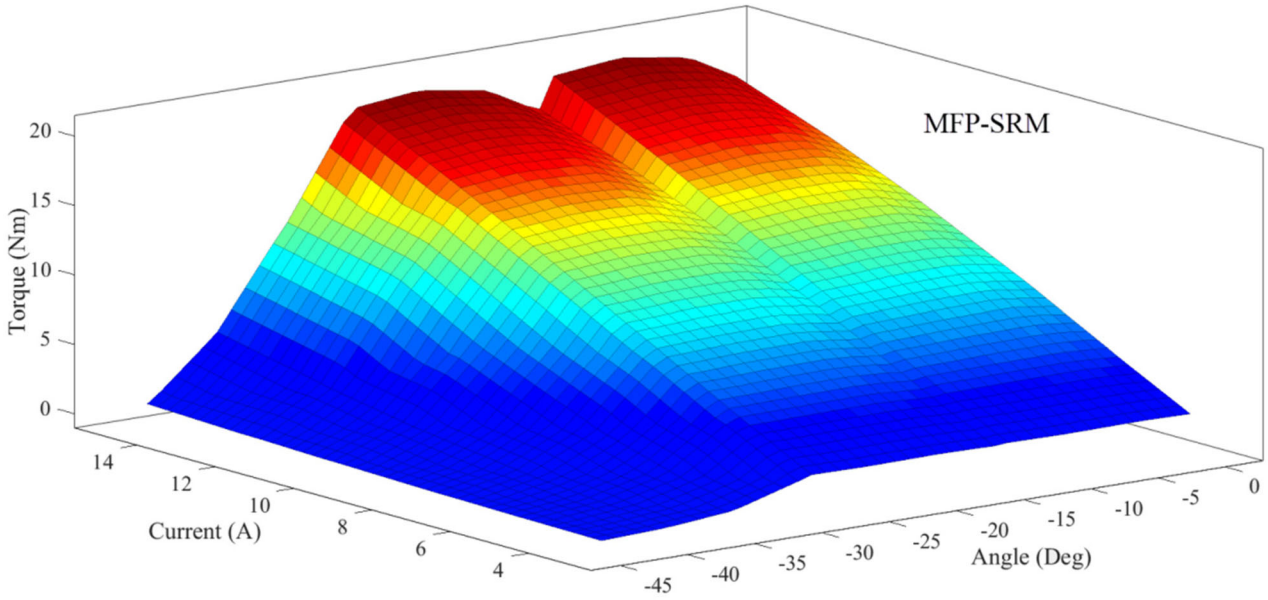

FIGURE 16. MFP-SRM angle–current–torque variation.

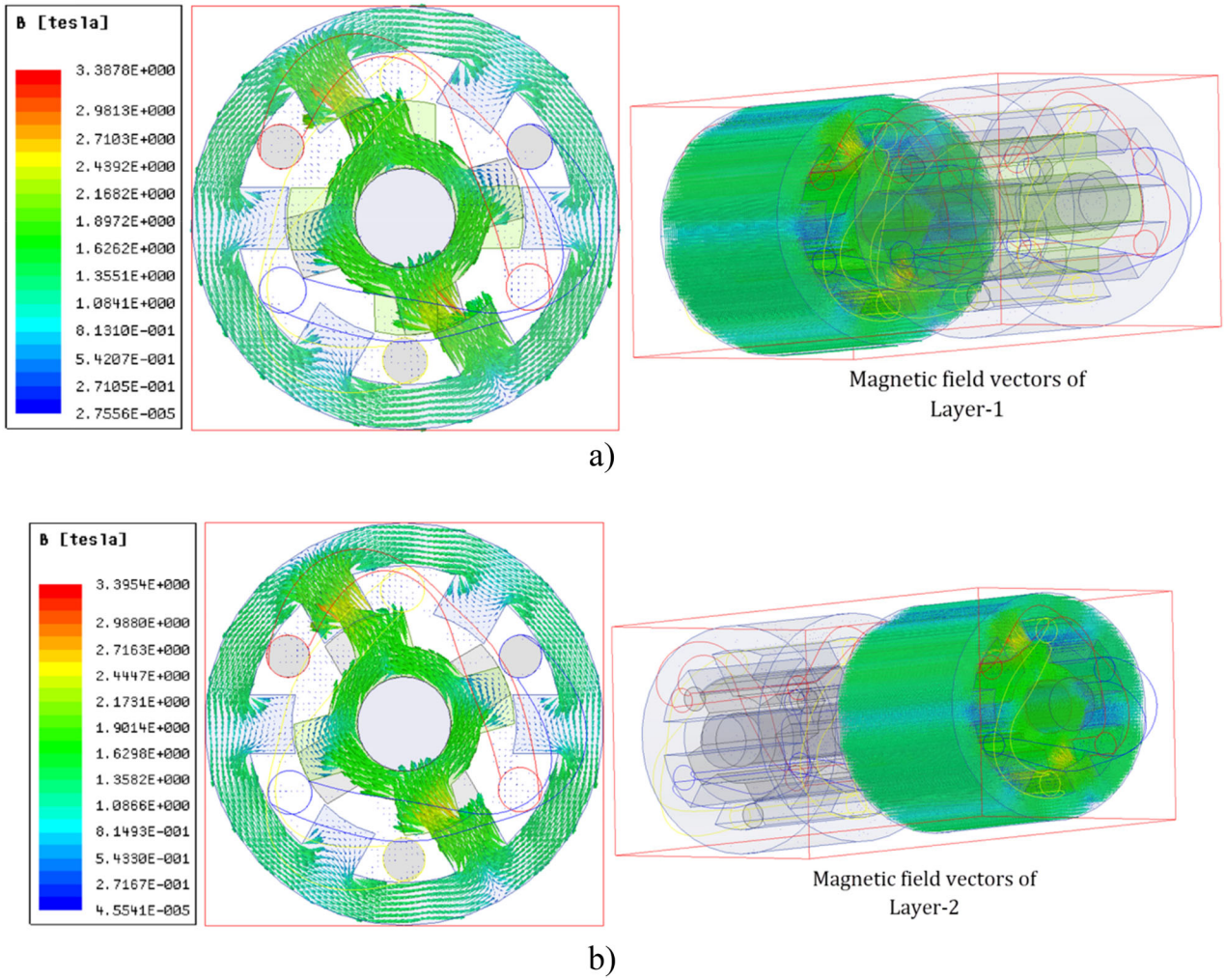

FIGURE 17. Magnetic field vectors: (a) Layer-1, (b) Layer-2.

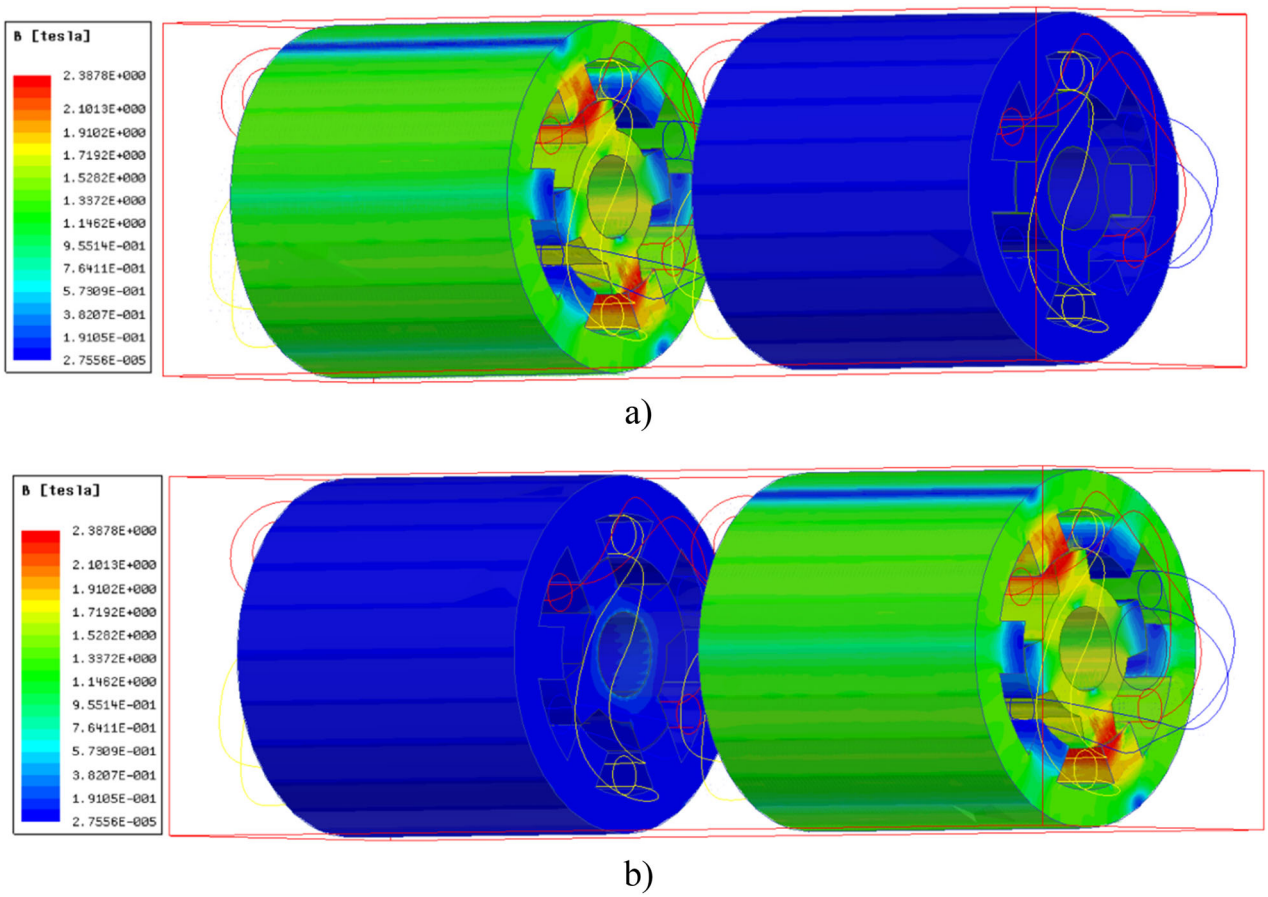

FIGURE 18. Magnetic flux density distribution: (a) Layer-1, (b) Layer-2.

layer are energized for torque generation and mutual inductance is produced between the phases. Figure 13 shows the mutual inductance curve obtained from the analysis results. The point to note in the curve is the mutual inductance profile obtained at the intervals where the layers contribute to the maximum torque generation.

Torque ripple is one of the most important parameters affecting the performance of electrical machines. In general, the minimum torque ripple is desired from electric motors. Because a high torque ripple negatively affects the motor output torque as well as causes high noise. Figure 14 shows the torque ripple of classical 6/4 FP-SRM.

The torque ripple of any electric machine can be calculated as given in Eq. (14) [49]:

$$Torque\ ripple\ (T_{rip}) = \frac{T_{ins(\max)} - T_{ins(\min)}}{T_{avg}} \tag{14}$$

Here, T_{max}, T_{min}, and T_{avg} denote the maximum, minimum, and average torque, respectively. The average torque expression is given in Eq. (15) as the integral of the instantaneous torque obtained over a period.

$$T_{avg} = \frac{1}{T}\int_0^T T_{inst}dt \tag{15}$$

The torque ripples of the classical FP-SRM (Figure 6) and MFP-SRM (Figure 12) were calculated with Eqs. (14) and (15). Torque, torque ripple, P_{out} and efficiency results are presented in Table 3.

As can be seen in Table 3, the torque ripple of the conventional FP-SRM varies between 31.99% and 38.19%, while the torque ripple of the MFP-SRM varies between 3.23% and 7.11%. As a result of the improvement in torque ripple, the average output torque increased between 27.61% and 33.16%. Figure 15 shows the comparison of the classical FP-SRM and the proposed model MFP-SRM output torque curves for 5,10 and 15 Amps, respectively.

As can be seen in Figure 15, when the torque curve of MFP-SRM and torque curves of FP-SRM are compared, it is seen that MFP-SRM offers a flatter and softer torque output with less torque ripple. The phase shift achieved by the α angle allows the rotor in the second layer to follow

the rotor in the first layer 15 degrees behind. In this way, in MFP-SRM, each layer contributes to the output torque only in the maximum torque regions. Figure 16 shows the angle–current–torque variation of the MFP-SRM in 3D.

Since both layers (Layer 1/Layer 2) are magnetically independent of each other and contribute to the torque generation in independent time intervals, their flux distributions are also independent of each other. Figure 17 shows the magnetic field vectors of Layer 1 and Layer 2 at 10 Amps. Figure 18 shows the magnetic flux density distribution of Layer 1 and Layer 2 at 10 Amps. There is a difference of 15° degrees between both rotor positions.

6. SUMMARY AND CONCLUSIONS

In this study, a multi-layer structure is presented to reduce the torque ripple of FP-SRMs. FP-SRMs, which have higher torque density compared to conventional SRMs, have a wider usage area with the improvements made in the torque ripple.

Especially the increase in the use of hybrid and electric vehicles and the developments in the aviation sector have bring higher performance expectations from the electric motor used. At this point, FP-SRMs with 20–30% higher torque density compared to traditional SRMs may be a good alternative. However, high torque ripple is a disadvantage for FP-SRMs. This situation is eliminated by geometric design and various control methods. It is applied to various motors in multi-layer structures to minimize the torque ripple.

In the literature studies given in Chapter 3; there are different studies such as the magnetic equivalent circuit model, hybrid structures with multi-layer structures for both motor and generator modes, and the effects of multi-layer structures on acoustic noise by reducing the torque ripple for multi-layer SRMs. In addition, it has been observed that the multi-layer structure reduces torque ripple in SRMs up to 23%. However, no fully pitched winding structure was used in any of the studies.

For this purpose, MFP-SRM design has been realized by combining the advantages of FP-SRM and multi-layer. The MFP-SRM structure for general use (Submersible pumps, electric vehicles, etc.) was designed as 3D, its magnetostatic analysis was performed, and the working area where the phase windings contributed the highest to the output torque was determined. Each layer of the two-layer MFP-SRM contributes to the output torque independently. Each layer contributes to the output torque at the maximum torque generating points. As a result of the analysis, it is observed that there is a decrease up to 34.16% in the torque ripple of MFP-SRM and an improvement up to 33.16% in the average output torque. In this way, MFP-SRM offers a smoother and ripple-free torque curve. In this regard, it is thought that it can be presented as an innovation to the literature and the interest in FP-SRMs with high performance will increase.

ORCID

Cihan Sahin http://orcid.org/0000-0002-3783-2260
Sinan Basaran http://orcid.org/0000-0001-6430-7827

REFERENCES

[1] H. Wang and F. Li, "Design consideration and characteristic investigation of modular permanent magnet bearingless switched reluctance motor," *IEEE Trans. Indus. Electron.*, vol. 67, no. 6, pp. 4326–4337, Jun. 2020. DOI: 10.1109/TIE.2019.2931218.

[2] W. Ding, Y. Hu, and L. Wu, "Analysis and development of novel three-phase hybrid magnetic paths switched reluctance motors using modular and segmental structures for EV applications," *IEEE/ASME Trans. Mech.*, vol. 20, no. 5, pp. 2437–2451, Oct. 2015. DOI: 10.1109/TMECH.2014.2383615.

[3] A. Shahabi, A. Rashidi, M. Afshoon, and S. M. Saghaian Nejad, "Commutation angles adjustment in SRM drives to reduce torque ripple below the motor base speed," *Turk. J. Elec. Eng. Comp. Sci.*, vol. 24, pp. 669–682, Jan. 2016. DOI: 10.3906/elk-1309-47.

[4] M. Tursini, M. Villani, G. Fabri, and L. Di Leonardo, "A switched-reluctance motor for aerospace application: Design, analysis and results," *Electr. Power Syst. Res.*, vol. 142, pp. 74–83, Sep. 2017. DOI: 10.1016/j.epsr.2016.08.044.

[5] M. Karacor, "Torque ripple reduction of mutually coupled reluctance motor," Ph.D. dissertation, Dept. Elec. Edu., Kocaeli Univ, 2010, Turkey.

[6] N. Kurihara, J. Bayless, H. Sugimoto, and A. Chiba, "Noise reduction of switched reluctance motor with high number of poles by novel simplified current waveform at low speed and low torque region," *IEEE Trans. Indus. Appl.*, vol. 52, no. 4, pp. 3013–3021, Jul.–Aug. 2016. DOI: 10.1109/TIA.2016.2549993.

[7] J. W. Jiang, B. Bilgin, and A. Emadi, "Three-phase 24/16 switched reluctance machine for a hybrid electric powertrain," *IEEE Trans. Transp. Electr.*, vol. 3, no. 1, pp. 76–85, Mar. 2017. DOI: 10.1109/TTE.2017.2664778.

[8] H. Ma, C. Huang, X. Liu, W. Shi, and W. Liu, "The effect of a single-sided pole shoe and slot on reducing torque ripple in a switched reluctance motor," *Concurr. Comput. Pract. Exp.*, vol. 32, no. 19, pp. e5810, May 2020. DOI: 10.1002/cpe.5810.

[9] D. Marcsa and M. Kuczmann, "Design and control for torque ripple reduction of a 3-phase switched reluctance motor," *Comput. Math. Appl.*, vol. 74, no. 1, pp. 89–95, Jul. 2017. DOI: 10.1016/j.camwa.2017.01.001.

[10] H.-S. Ro, K.-G. Lee, J.-S. Lee, H.-G. Jeong, and K.-B. Lee, "Torque ripple minimization scheme using torque sharing function based fuzzy logic control for a switched reluctance motor," *J. Electr. Eng. Technol.*, vol. 10, no. 1, pp. 118–127, Jan. 2015. DOI: 10.5370/JEET.2015.10.1.118.

[11] X. Y. Ma, G. J. Li, G. W. Jewell, Z. Q. Zhu, and H. L. Zhan, "Performance comparison of doubly salient reluctance machine topologies supplied by sinewave currents," *IEEE Trans. Indus. Electr.*, vol. 63, no. 7, pp. 4086–4096, Jul. 2016. DOI: 10.1109/TIE.2016.2544722.

[12] X. Deng, B. Mecrow, H. Wu, and R. Martin, "Design and development of low torque ripple variable-speed drive system with six-phase switched reluctance motors," *IEEE Trans. Energy Convers.*, vol. 33, no. 1, pp. 420–429, Mar. 2018. DOI: 10.1109/TEC.2017.2753286.

[13] H. Ishikawa, T. Imai, and H. Naitoh, "New drive circuit for reducing the switching current ripples in switched reluctance motors," *Electr. Eng. Jpn.*, vol. 203, no. 2, pp. 47–57, Oct. 2018. DOI: 10.1002/eej.23075.

[14] Q. Sun, J. Wu, C. Gan, Y. Hu, and J. Si, "OCTSF for torque ripple minimisation in SRMs," *IET Power Electr.*, vol. 9, no. 14, pp. 2741–2750, Nov. 2016. DOI: 10.1049/iet-pel.2016.0270.

[15] E. Daryabeigi, M. M. Namazi, A. Emanian, A. Rashidi, and S. M. Saghaian-Nejad, "Torque ripple reduction of switched reluctance motor (SRM) drives, with emotional controller (BELBIC)," in *Proc. 2012 Twenty-Seventh Annual IEEE Applied Pwr. Elec. Conf. and Exposition (APEC)*, 2012. pp. 1528–1535. DOI: 10.1109/APEC.2012.6166023.

[16] M. A. Kabir and I. Husain, "Design of mutually coupled switched reluctance motors (MCSRMs) for extended speed applications using 3-phase standard inverters," *IEEE Trans. Energy Convers.*, vol. 31, no. 2, pp. 436–445, Jun. 2016. DOI: 10.1109/TEC.2015.2499086.

[17] P. Azer, B. Bilgin, and A. Emadi, "Mutually coupled switched reluctance motor: Fundamentals, control, modeling, state of the art review and future trends," *IEEE Access*, vol. 7, pp. 100099–100112, Jul. 2019. DOI: 10.1109/ACCESS.2019.2930895.

[18] B. C. Mecrow, "Fully pitched-winding switched-reluctance and stepping-motor arrangements," *IEE Proc. B Electr. Power Appl. UK*, vol. 140, no. 1, pp. 61–70, Jan. 1993. DOI: 10.1049/ip-b.1993.0008.

[19] A. Clothier and B. C. Mecrow, "Inverter topologies and current sensing methods for short pitched and fully pitched winding SR motors," in *Proc. Fourteenth Annual Applied Power Electronics Conference and Exposition (APEC'99)*, 1999. DOI: 10.1109/APEC.1999.749711.

[20] B. C. Mecrow, "New winding configurations for doubly salient reluctance machines," *IEEE Trans. Indus. Appl.*, vol. 32, no. 6, pp. 1348–1356, Nov.–Dec. 1996. DOI: 10.1109/28.556638.

[21] E. Sayed, M. H. Bakr, B. Bilgin, and A. Emadi, "Adjoint sensitivity analysis of switched reluctance motors," *Electr. Power Compon. Syst.*, vol. 46, no. 18, pp. 1959–1968, Dec. 2018. DOI: 10.1080/15325008.2018.1531326.

[22] R. Alipour-Sarabi, Z. Nasiri-Gheidari, and H. Oraee, "Development of a three-dimensional magnetic equivalent circuit model for axial flux machines," *IEEE Trans. Indus. Electr.*, vol. 67, no. 7, pp. 5758–5767, Jul. 2020. DOI: 10.1109/TIE.2019.2934065.

[23] C. Sahin, A. E. Amac, M. Karacor, and A. Emadi, "Reducing torque ripple of switched reluctance machines by relocation of rotor moulding clinches," *IET Electr. Power Appl.*, vol. 6, no. 9, pp. 753, Nov. 2012. DOI: 10.1049/iet-epa.2011.0397.

[24] Sun, S. Wang, Z. Kuang, and H. Wu, "Torque ripple comparison of short-pitched and fully-pitched winding switched reluctance machine," in *Proc. 2012 15th Inter. Conf. on Elec. Mach. and Syst. (ICEMS)*, 2012, pp. 1–6.

[25] K. Yilmaz and S. Sezen, "Performance analysis between short pitched and fully pitched sr motors with computed phase resistance value based on 3-d parametric design," *J. Fac. Eng. Arch. Gazi Univ.*, vol. 28, no. 2, pp. 375–384, Jun. 2008.

[26] Y. Lan, et al., "Switched reluctance motors and drive systems for electric vehicle powertrains: State of the art analysis and future trends," *Energies*, vol. 14, no. 8, pp. 2079, 2021. DOI: 10.3390/en14082079.

[27] A. Seshadri and N. C. Lenin, "Review based on losses, torque ripple, vibration and noise in switched reluctance motor," *IET Electr. Power Appl.*, vol. 14, no. 8, pp. 1311–1326, 2020. DOI: 10.1049/iet-epa.2019.0251.

[28] P. Vahedi, B. Ganji, and E. Afjei, "Multi-layer switched reluctance motors: Performance prediction and torque ripple reduction," *Int. Trans. Electr. Energ Syst.*, vol. 30, no. 2, pp. e12215, Nov. 2020. DOI: 10.1002/2050-7038.12215.

[29] A. Siadatan, H. Torkaman, and A. Afjei, "Septi-Segment switched reluctance machine: Design, modeling, and nanufacturing," *Int. Trans. Electr. Energ. Syst.*, vol. 26, no. 8, pp. 1673–1684, Dec. 2016. DOI: 10.1002/etep.2170.

[30] E. Afjei, A. Siadatan, and H. Torkaman, "Magnetic modeling, prototyping, and comparative study of a quintuple-set switched reluctance motor," *IEEE Trans. Magn.*, vol. 51, no. 8, pp. 1–7, Aug. 2015. DOI: 10.1109/TMAG.2015.2418257.

[31] A. Siadatan, E. Afjei, H. Torkaman, and M. Rafie, "Design, simulation and experimental results for a novel type of two-layer 6/4 three-phase switched reluctance motor/generator," *Energy Convers. Manage.*, vol. 71, pp. 199–207, Jul. 2013. DOI: 10.1016/j.enconman.2013.03.011.

[32] S. E. Afjei, A. Siadatan and H. Torkaman, "Analytical design and fem verification of a novel three-phase seven layers switched reluctance motor," *PIER*, vol. 140, pp. 131–146, May 2013. DOI: 10.2528/PIER13040705.

[33] H. Torkaman, E. Afjei and M. S. Toulabi, "New double-layer-per-phase isolated switched reluctance motor: Concept, numerical analysis, and experimental confirmation," *IEEE Trans. Indus. Electron*, vol. 59, no. 2, pp. 830–838, Feb. 2012. DOI: 10.1109/TIE.2011.2158049.

[34] F. Daldaban and N. Ustkoyuncu, "Multi-layer switched reluctance motor to reduce torque ripple," *Energy Convers. Manage.*, vol. 49, no. 5, pp. 974–979, May 2008. DOI: 10.1016/j.enconman.2007.10.011.

[35] E. S. Afjei and H. A. Toliyat, "A novel multilayer switched reluctance motor," *IEEE Trans. Energy Convers.*, vol. 17, no. 2, pp. 217–221, Jun. 2002. DOI: 10.1109/TEC.2002.1009471.

[36] P. Vahedi, B. Ganji, and E. Afjei, "A multi-physics simulation model based on finite element method for the multi-layer switched reluctance motor," *Iran. J. Elect. Electr. Eng.*, vol. 16, no. 4, pp. 494–504, Dec. 2020. DOI: 10.22068/IJEEE.16.4.494.

[37] S. Muruganantham and R. Ashokkumar, "A novel six layered switched reluctance motor with IGBT controller design for torque improvement and torque ripple reduction," *Int. J. Appl. Eng. Res.*, vol. 13, no. 15, pp. 11839–11843, 2018.

[38] A. Siadatan, M. M. Mahmoodi, and M. M. Nezamabad, "Torque comparison between a novel multilayer switched reluctance motor and a custom one," *Res. J. Recent Sci.*, vol. 5, no. 2, pp. 56–65, Feb. 2016.

[39] A. Siadatan and E. Afjei, "An 8/6 two layers switched reluctance motor: Modeling, simulation and experimental analysis," *Majlesi J. Electr. Eng.*, vol. 6, no. 1, pp. 1–10, Mar. 2012.

[40] W. A. Arakat, A. Y. Haikal and A. H. Kassem, "Adaptive neuro-fuzzy controller for multi-layered switched reluctance motor," *IJCA*, vol. 44, no. 1, pp. 20–25, Apr. 2012. DOI: 10.5120/6228-8304.

[41] E. Afjei and A. Siadatan, "A novel two phase hybrid switched reluctance motor/field-assisted generator: Concept, simulation, and experimental confirmation," *IJE Trans. B: Appl.*, vol. 22, no. 4, pp. 357–368, Dec. 2009.

[42] H. Arihara and K. Akatsu, "Basic properties of an axial-type switched reluctance motor," *IEEE Trans. Indus. Appl.*, vol. 49, no. 1, pp. 59–65, Jan.–Feb. 2013. DOI: 10.1109/TIA.2012.2229683.

[43] M. Karacor and F. E. Kuyumcu, "Matlab GUI based SRM design program," in *2007 International Aegean Conference on Electrical Machines and Power Electronics*, 2007. DOI: 10.1109/ACEMP.2007.4510570.

[44] Z. Zhang, S. Rao, and X. Zhang, "Performance prediction of switched reluctance motor using improved generalized regression neural networks for design optimization," *Trans. Electr. Mach. Syst.*, vol. 2, no. 4, pp. 371–376, Dec. 2018. DOI: 10.30941/CESTEMS.2018.00047.

[45] T. Lambert, M. Biglarbegian and S. Mahmud, "A novel approach to the design of axial-flux switched-reluctance motors," *Machines*, vol. 3, no. 1, pp. 27–54, Mar. 2015. DOI: 10.3390/machines3010027.

[46] P. N. Kumar and T. Isha, "Inductance calculation of 8/6 switched reluctance motor," in *Joint International Conference on Power System Technology and IEEE Power India Conference*, 2008, pp. 1–5. DOI: 10.1109/ICPST.2008.4745325.

[47] B.-H. Nguyen and C.-M. Ta, "Finite element analysis, modeling and torque distribution control for switched reluctance motors with high non-linear inductance characteristics," in 2011 IEEE International Electric Machines & *Drives Conference (IEMDC)*, 2011, pp. 693–698. DOI: 10.1109/IEMDC.2011.5994895.

[48] K. Kiyota, S. Nakano, and A. Chiba, "A fast calculation method of optimal ratio of outer diameter and axial length for torque improvement in switched reluctance motor," *IEEE Trans. Indus. Appli.*, vol. 54, no. 6, pp. 5802–5811, Nov.–Dec. 2018. DOI: 10.1109/TIA.2018.2850024.

[49] T. Mohanarajah, J. Rizk, M. Nagrial, and A. Hellany, "Finite element analysis and design methodology for high-efficiency synchronous reluctance motors," *Electr. Power Compon. Syst.*, vol. 46, no. 13, pp. 1478–1493, Nov. 2018. DOI: 10.1080/15325008.2018.1489436.

BIOGRAPHIES

Cihan Sahin received his M.S. and Ph.D. degrees in Electrical Education from Kocaeli University, Kocaeli, Turkey, in 2007 and 2014, respectively. His research interests are automation systems, power electronics, and electric machines design and applications.

Sinan Basaran received his M.S. degrees in Mechanical Engineering from Gebze Institute of Technology, Kocaeli, Turkey in 2011 and Ph. D. degrees in Mechanical Engineering from Gebze Technical University, Gebze, Turkey in 2017. His research interests are magnetic levitation systems, vibration control, and mechatronics system design and applications.